Supplementary Information (SI) for CrystEngComm.

Supporting Information

Interplay of C–H···F and halogen bonding interactions for tunable room-temperature phosphorescence in iododiphenylacetylene systems

Masato Morita,*[a] Motohiro Yasui,[b] Tsutomu Konno [b] and Shigeyuki Yamada *[b]

a. Graduate School of Science and Engineering, Ibaraki University, 4-12-1 Nakanarusawa, Hitachi, Ibaraki 316-8511, Japan.

b. Faculty of Molecular Chemistry and Engineering, Kyoto Institute of Technology, Matsugasaki, Sakyo-ku, Kyoto 606-8585, Japan.

E-mail: syamada@kit.ac.jp

Contents

1. Experimental ____ S-1

2. ^{1}H and ^{19}F NMR spectra ____ S-3

3. PL spectra ____ S-5

4. Single-crystal X-ray diffraction ____ S-8

5. Quantum chemical calculation ____ S-15

1. Experimental

Materials and Methods

The ^{1}H-NMR (400 MHz) and ^{13}C-NMR (100 MHz) spectra were obtained using a Bruker AVANCE III 400 NMR spectrometer in a chloroform-*d* ($CDCl_3$) solution. The chemical shifts were reported in parts per million (ppm) using residual protons in the NMR solvent. The ^{19}F-NMR (376 MHz) spectra were obtained using a Bruker AVANCE III 400 NMR spectrometer in a $CDCl_3$ solution with $CFCl_3$ (δ_F = 0 ppm) as the internal standard. All chemicals, including the solvents, were of reagent grade and purified as typical prior to use. Column chromatography was conducted on silica gel (Fujifilm Wako Pure Chemical Corporation, Wakogel® 60 N, 38–100 μm), and thin-layer chromatography (TLC) was performed on silica gel TLC plates (Merck, Silica gel 60F_{254}).

General procedure of the Sonogashira cross-coupling reaction

The phenylacetylene derivative, aromatic iodide (1.2 eq.), $Cl_2Pd(PPh_3)_2$ (5 mol%), PPh_3 (5 mol%), CuI (10 mol%), and Et_3N were placed in a flask, and the suspended solution was stirred overnight at 60 °C. Following reaction completion, the resulting precipitate was separated using atmospheric filtration. The filtrate was poured into a saturated aqueous NH_4Cl solution, and the crude product was extracted thrice using AcOEt. The collected organic layer was dried over anhydrous Na_2SO_4 and separated using atmospheric filtration. The filtrate was evaporated under vacuum and subjected to silica-gel column chromatography to obtain the desired products.

Preparation of 1-iodo-4-(phenylethynyl)benzene (2a)

Yield: 43% (white solid); ^{1}H-NMR ($CDCl_3$): δ 7.25–7.27 (m, 2H), 7.35–7.37 (m, 3H), 7.51–7.54 (m, 2H), 7.68–7.71 (m, 2H). The NMR data were consistent with the spectral data described in the previous literature.[1]

Preparation of 1-iodo-4-((4-methoxyphenyl)ethynyl)benzene (2b)

Yield: 32% (white solid); ^{1}H-NMR ($CDCl_3$): δ 3.83 (s, 3H), 6.88 (d, J = 8.9 Hz, 2H), 7.23 (d, J = 8.4 Hz, 2H), 7.46 (d, J = 8.9 Hz, 2H), 7.67 (d, J = 8.4 Hz, 2H). The NMR data were consistent with the spectral data described in the previous literature.[2]

[1] H. Li, D. R. Powell, T. K. Firman and R. West, *Macromolecules*, 1998, **31**, 1093–1098. https://doi.org/10.1021/ma971126s

[2] M. Irfan, I. Sumra, M. Zhang, Z. Song, T. Liu and Z. Zeng, *Dyes Pigm.*, 2021, **190**, 109272. https://doi.org/10.1016/j.dyepig.2021.109272

Preparation of 1,2,4,5-tetrafluoro-3-iodo-6-(phenylethynyl)benzene (2c)

Yield: 26% (white solid); ^{1}H-NMR ($CDCl_3$): δ 7.37–7.43 (m, 3H), 7.59–7.61 (d, J = 8.9 Hz, 2H); ^{19}F-NMR ($CDCl_3$): δ –121.65 to –121.73 (m, 2F), –136.08 to –136.16 (m, 2F). The NMR data were consistent with the spectral data described in the previous literature.[3]

[3] J. C. Collings, J. M. Burke, P. S. Smith, A. S. Batsanov, J. A. K. Howard and T. B. Marder, *Org. Biomol. Chem.*, 2004, **2**, 3172–3178. https://doi.org/10.1039/b411191e

2. ^{1}H and ^{19}F NMR spectra

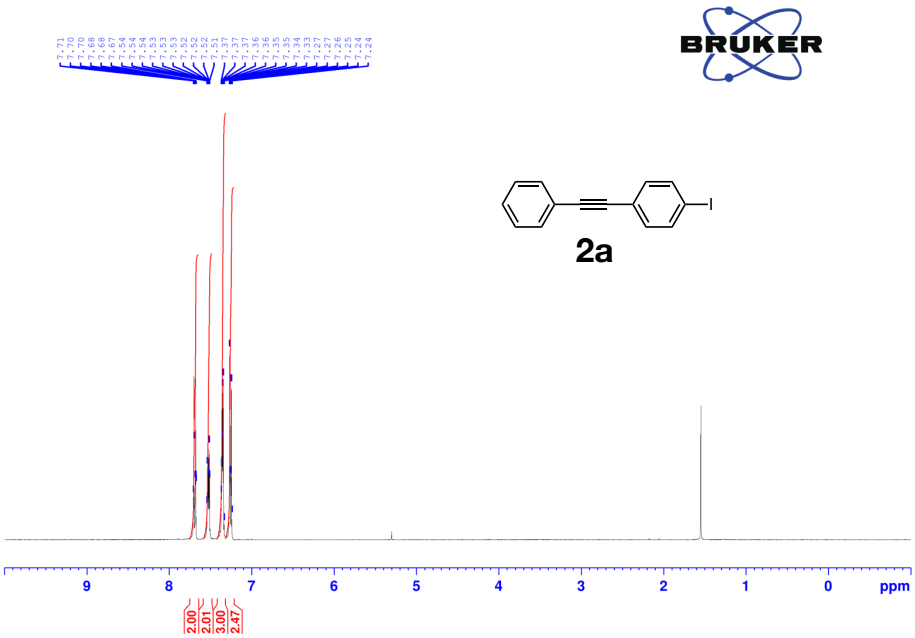

Fig. S1 ^{1}H NMR spectrum of **2a**.

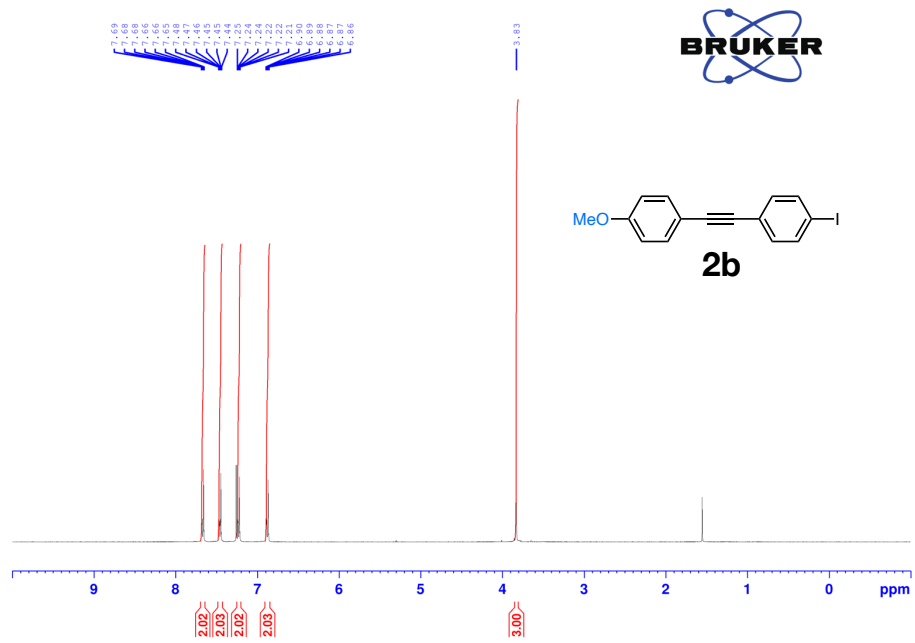

Fig. S2 ^{1}H NMR spectrum of **2b**.

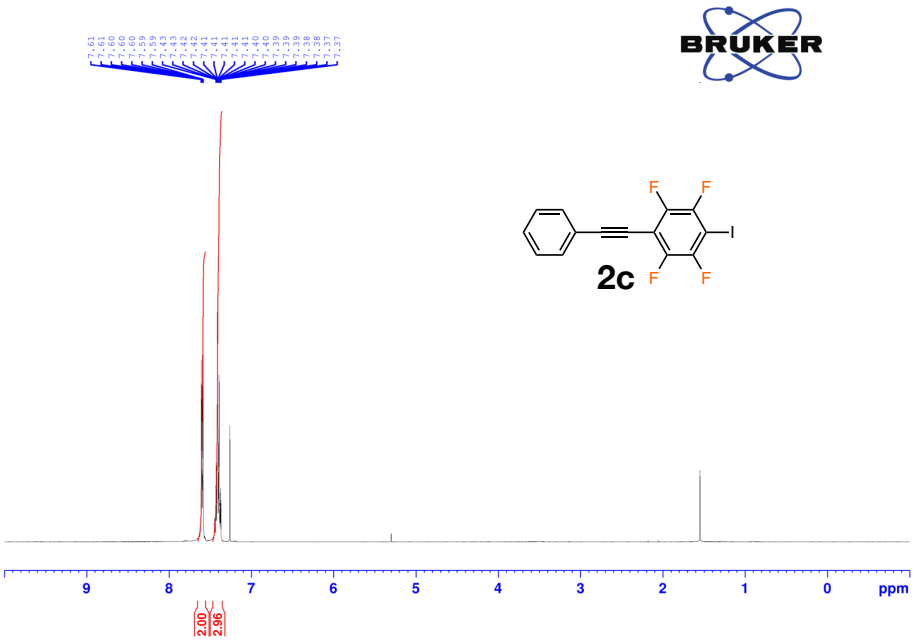

Fig. S3 ^{1}H NMR spectrum of **2c**.

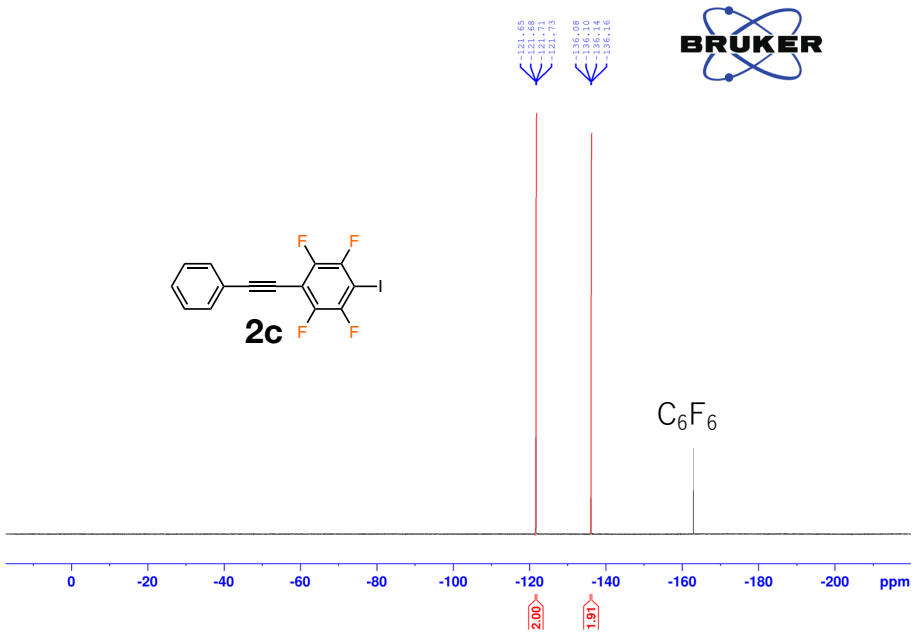

Fig. S4 ^{19}F NMR spectrum of **2c**.

3. PL spectra

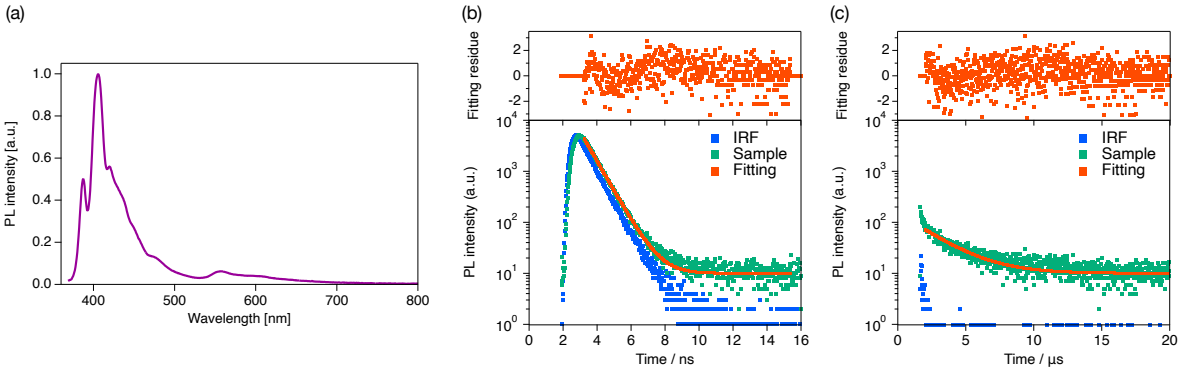

Fig. S5 PL profiles of **2a** (a) PL spectra, (b) PL decay curve monitored at 387 nm, (c) PL decay curve monitored at 559 nm with 350 nm excitation.

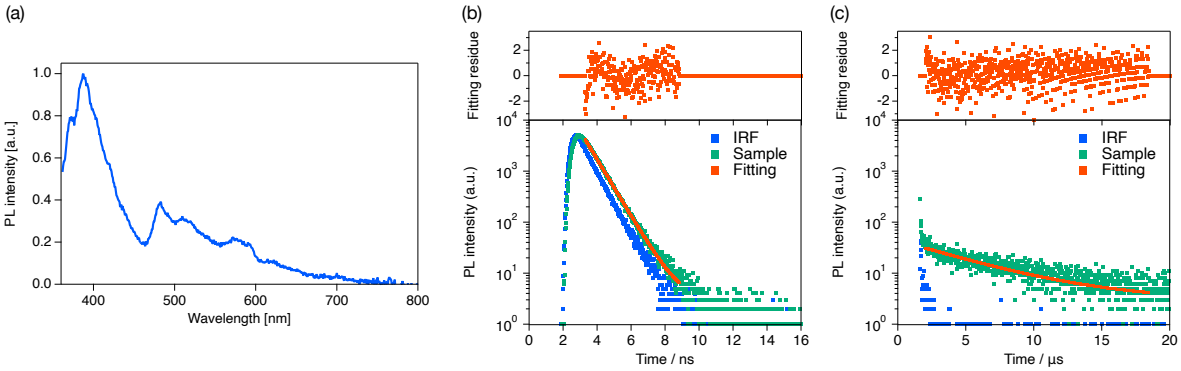

Fig. S6 PL profiles of **2b** (a) PL spectra, (b) PL decay curve monitored at 387 nm, (c) PL decay curve monitored at 581 nm with 350 nm excitation.

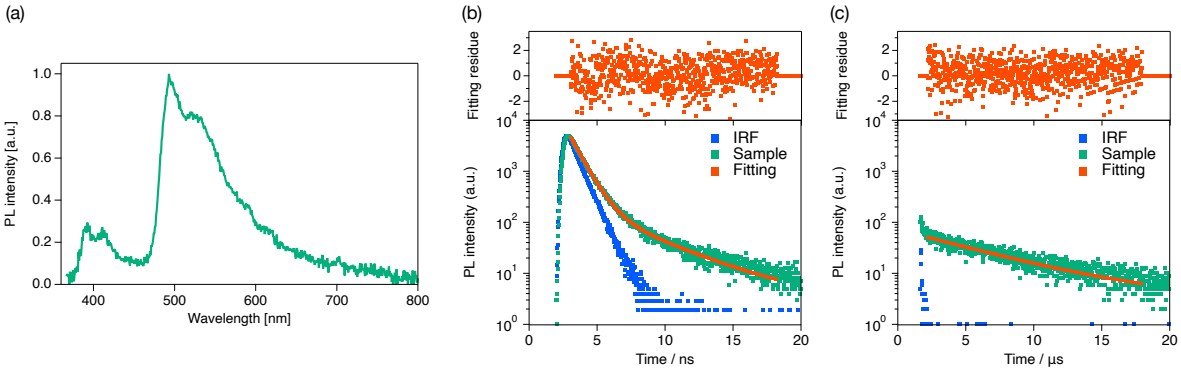

Fig. S7 PL profiles of **2c** (a) PL spectra, (b) PL decay curve monitored at 392 nm, (c) PL decay curve monitored at 493 nm with 350 nm excitation.

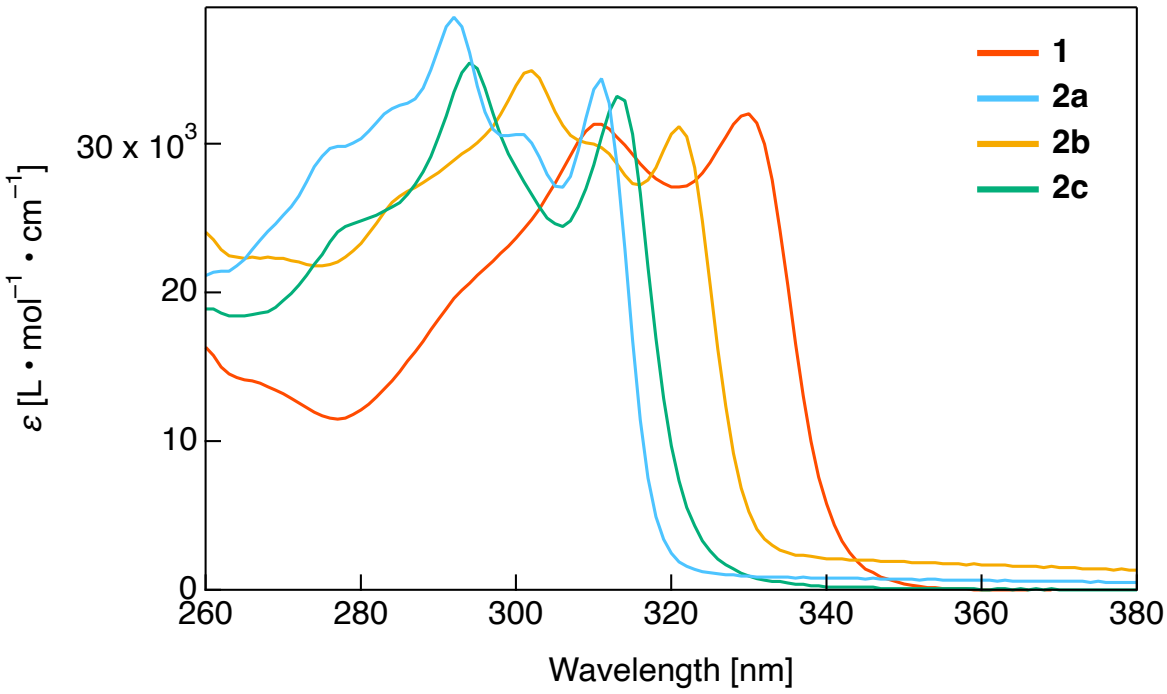

Fig. S8 UV/vis absorption spectra of **1**, **2a–c** in 10^{-5} mol L^{-1} CCl_4 solution.

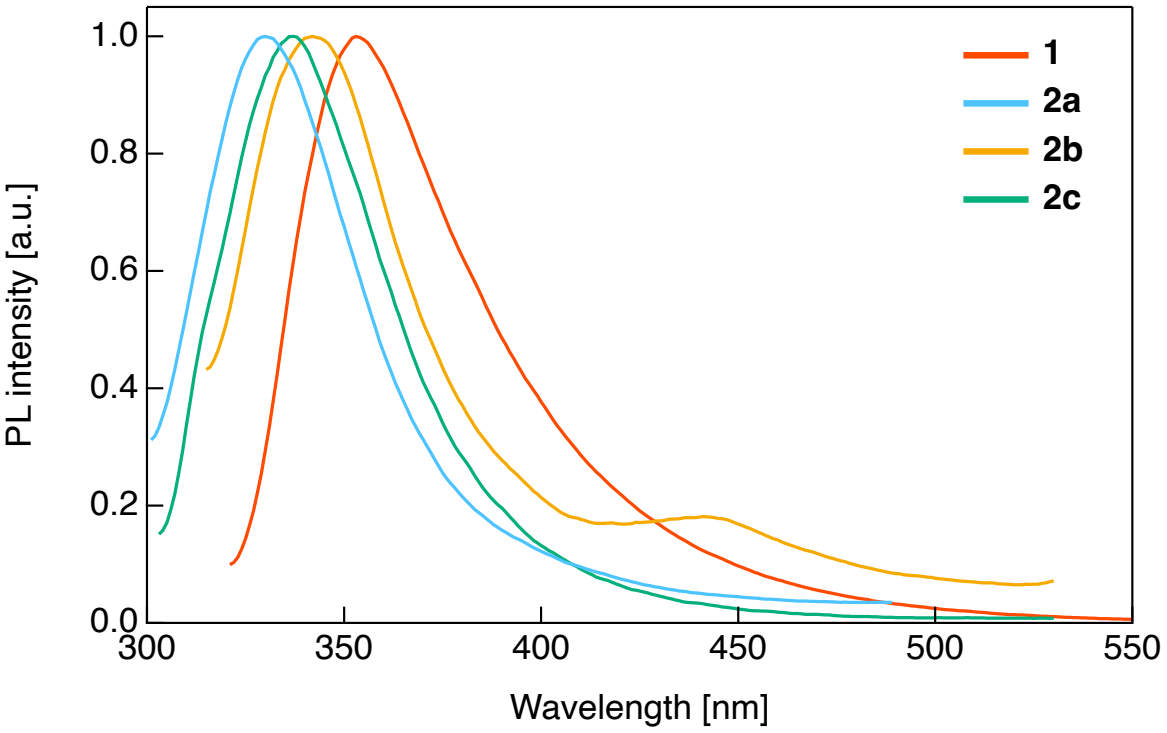

Fig. S9 PL spectra of **1**, **2a–c** excited at absorption maxima in 10^{-5} mol L^{-1} CCl_4 solution.

Table S1 Photophysical properties of **1**, **2a–c** in 10^{-5} mol L^{-1} CCl_4 solution.

	λ_{abs} [nm] (ε [L mol^{-1} cm^{-1}])	λ_{PL} [nm][a]	Φ_{PL}[b]
1	311 (31.3), 330 (32.0)	353	0.03
2a	292 (38.5), 311 (34.4)	330	0.02
2b	302 (34.9), 321 (31.2)	342	0.02
2c	294 (35.4), 313 (33.2)	337	0.02

a: excited at λ_{abs}, b: calculated using an integrating sphere.

4. Single-crystal X-ray diffraction

A Note on the Space Group Assignment for Compound 2a

The crystal structure of **2a** was previously reported in the space group *Pnma* (CCDC 1415296, 1575576). However, the diffraction data collected for the single crystal in this study did not satisfy the systematic absence conditions required for *Pnma*.

The *Pnma* space group requires systematic absences for 0*kl* reflections when *k*+*l* is odd and for *hk*0 reflections when *h* is odd. In our dataset, several reflections violating these conditions were clearly observed with significant intensities (I > 2σ(I)). Representative examples are listed below:

- **Observed reflections violating *Pnma* conditions:**
    - (0 4 1) (I/σ(I) = 44.5) (*violates k+l=2n rule*)
    - (0 2 3) (I/σ(I) = 32.1) (*violates k+l=2n rule*)
    - (1 2 0) (I/σ(I) = 28.7) (*violates h=2n rule*)
    - (5 2 0) (I/σ(I) = 20.8) (*violates h=2n rule*)

The definitive presence of these reflections proves that the *n*- and *a*-glide planes, which are essential symmetry elements of *Pnma*, are absent in our crystal. Therefore, higher symmetry space groups were ruled out, and the space group *P*2 was determined to be the most appropriate choice consistent with the observed diffraction data.

Table S2 Observed intensities for reflections of compound **2a** that should be systematically absent in the *Pnma* space group.

h	k	l	violated condition for *Pnma*	Int_{obs}	σ (Int_{obs})	Int_{obs}/ σ(Int_{obs})
0	4	1	k + l = odd	14437.95	324.50	44.49
0	2	3	k + l = odd	8416.20	262.44	32.07
1	2	0	h = odd	581.28	20.29	28.65
5	2	0	h = odd	2547.56	122.24	20.84

h, k, l are the Miller indices of the reflection. Int_{obs} is the observed intensity, σ(Int_{obs}) is its standard uncertainty, and Int_{obs}/ σ(Int_{obs}) is the resulting signal-to-noise ratio.

Table S3 Crystallographic data of **2a**, **2b**, and **2c**.

	2a	**2b**	**2c**
Chemical formula	$C_{14}H_9I$	$C_{15}H_{11}IO$	$C_{14}H_5F_4I$
M_r	304.11	334.14	376.08
Crystal system, space group	Monoclinic, *P*2	Orthorhombic, $Pca2_1$	Monoclinic, $P2_1/n$
Temperature (K)	298	298	298
a, *b*, *c* (Å)	7.5797(4), 5.9809(4), 52.204(3)	6.1455 (2), 7.4012 (3), 28.5289 (11)	12.9207 (9), 5.0801 (4), 19.1219 (11)
β (°)	91.697(4)	90	94.046 (6)
V (Å^3)	2365.6 (2)	1297.61 (8)	1252.00 (15)
Z	8	4	4
Radiation type	Mo *K*α	Mo *K*α	Mo *K*α
Crystal size (mm)	0.50 × 0.31 × 0.19	0.45 × 0.37 × 0.20	0.59 × 0.32 × 0.14
$R[F^2 > 2\sigma(F^2)]$, $wR(F^2)$, *S*	0.065, 0.199, 1.03	0.025, 0.066, 1.05	0.035, 0.096, 1.06

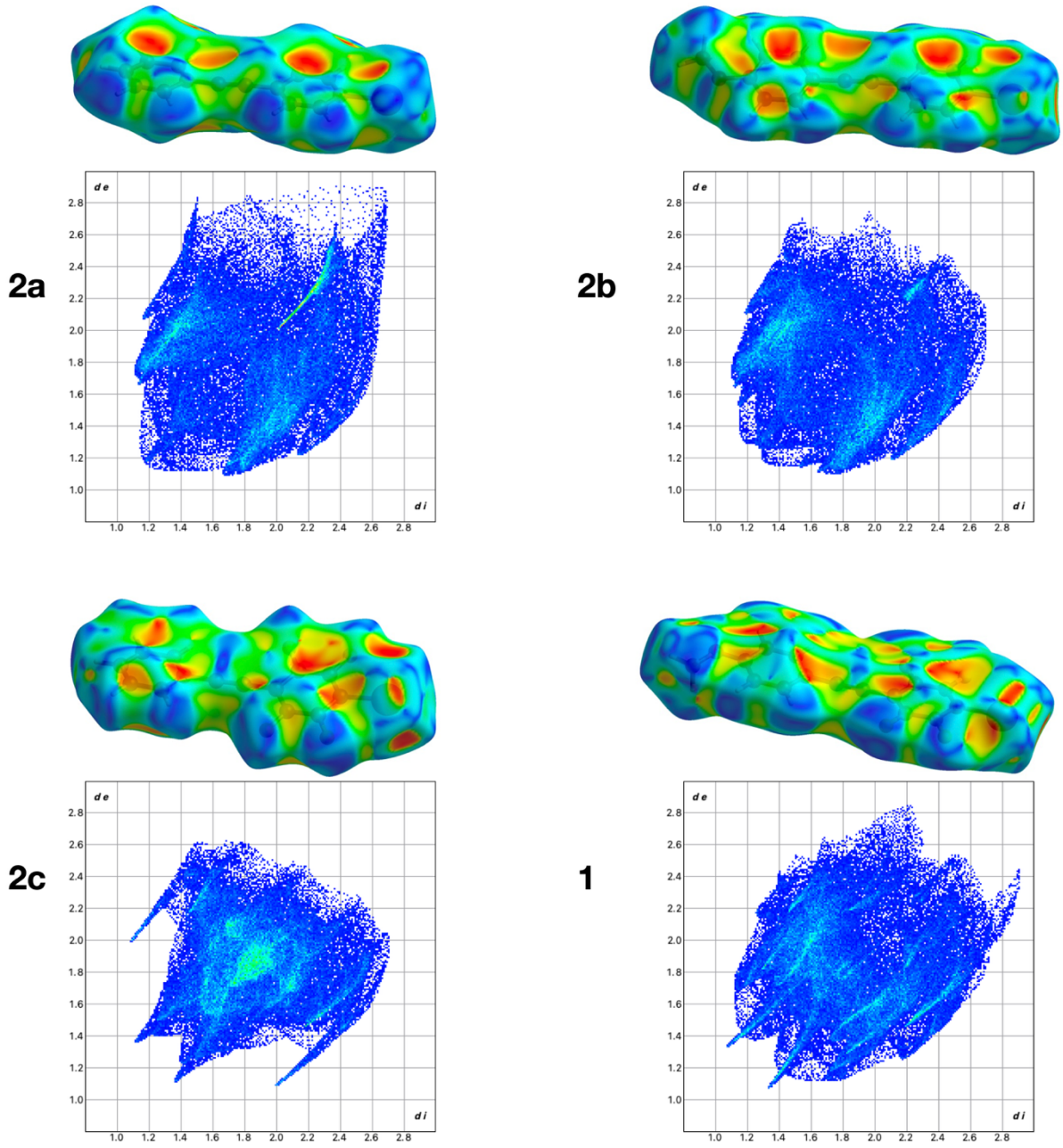

Fig. S10 Hirshfeld surface analysis for compounds **1**, **2a–c**. For each compound, the shape index (top) and the full 2D fingerprint plot (bottom) are shown.

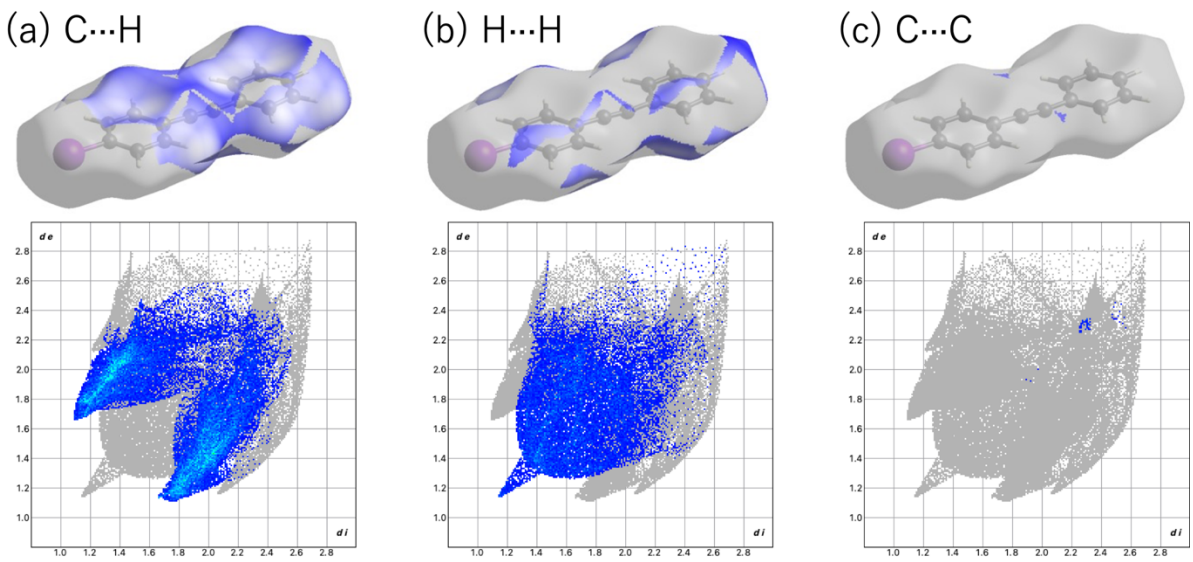

Fig. S11 Decomposed 2D Hirshfeld fingerprint plots for compound **2a**, illustrating the contributions from the principal intermolecular contacts: (a) C···H, (b) H···H, and (c) C···C. The Hirshfeld surfaces above each plot are mapped with d_{norm} to highlight the areas corresponding to each specific contact.

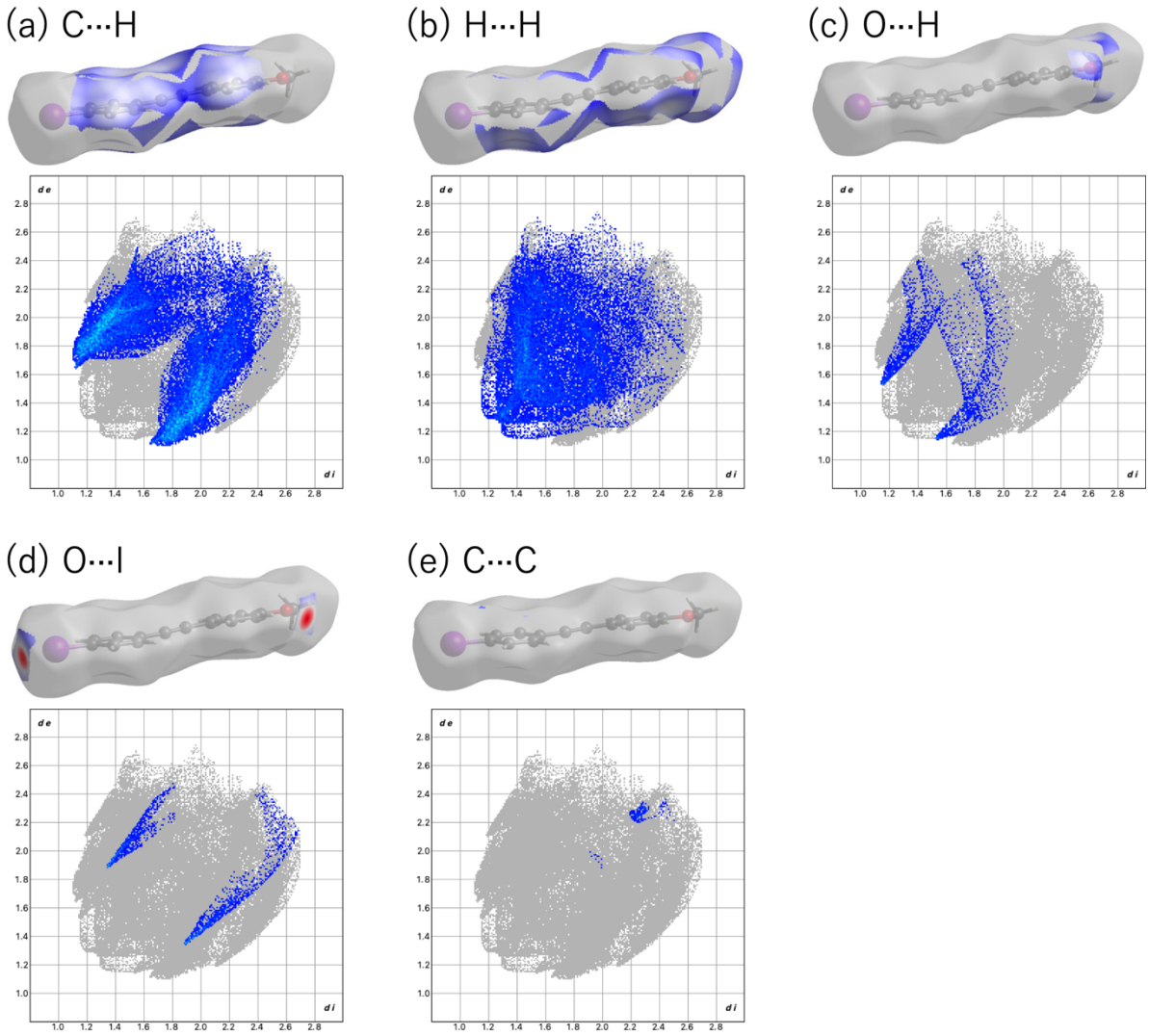

Fig. S12 Decomposed 2D Hirshfeld fingerprint plots for compound **2b**, illustrating the contributions from the principal intermolecular contacts: (a) C···H, (b) H···H, (c) O···H, (d) O···I, and (e) C···C. The Hirshfeld surfaces above each plot are mapped with d_{norm} to highlight the areas corresponding to each specific contact.

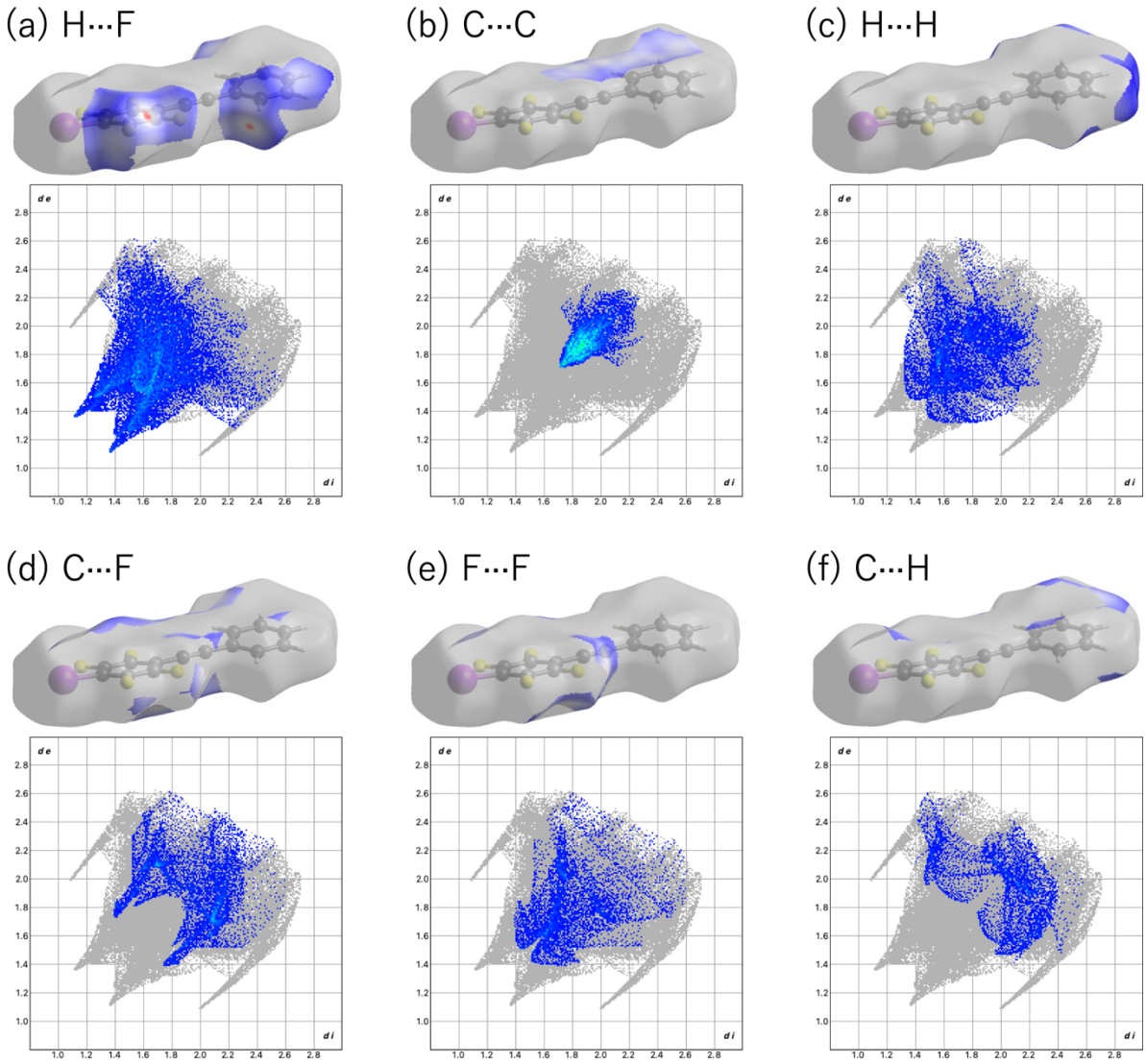

Fig. S13 Decomposed 2D Hirshfeld fingerprint plots for compound **2c**, illustrating the contributions from the principal intermolecular contacts: (a) H···F, (b) C···C, (c) H···H, (d) C···F, (e) F···F, and (f) C···H. The Hirshfeld surfaces above each plot are mapped with d_{norm} to highlight the areas corresponding to each specific contact.

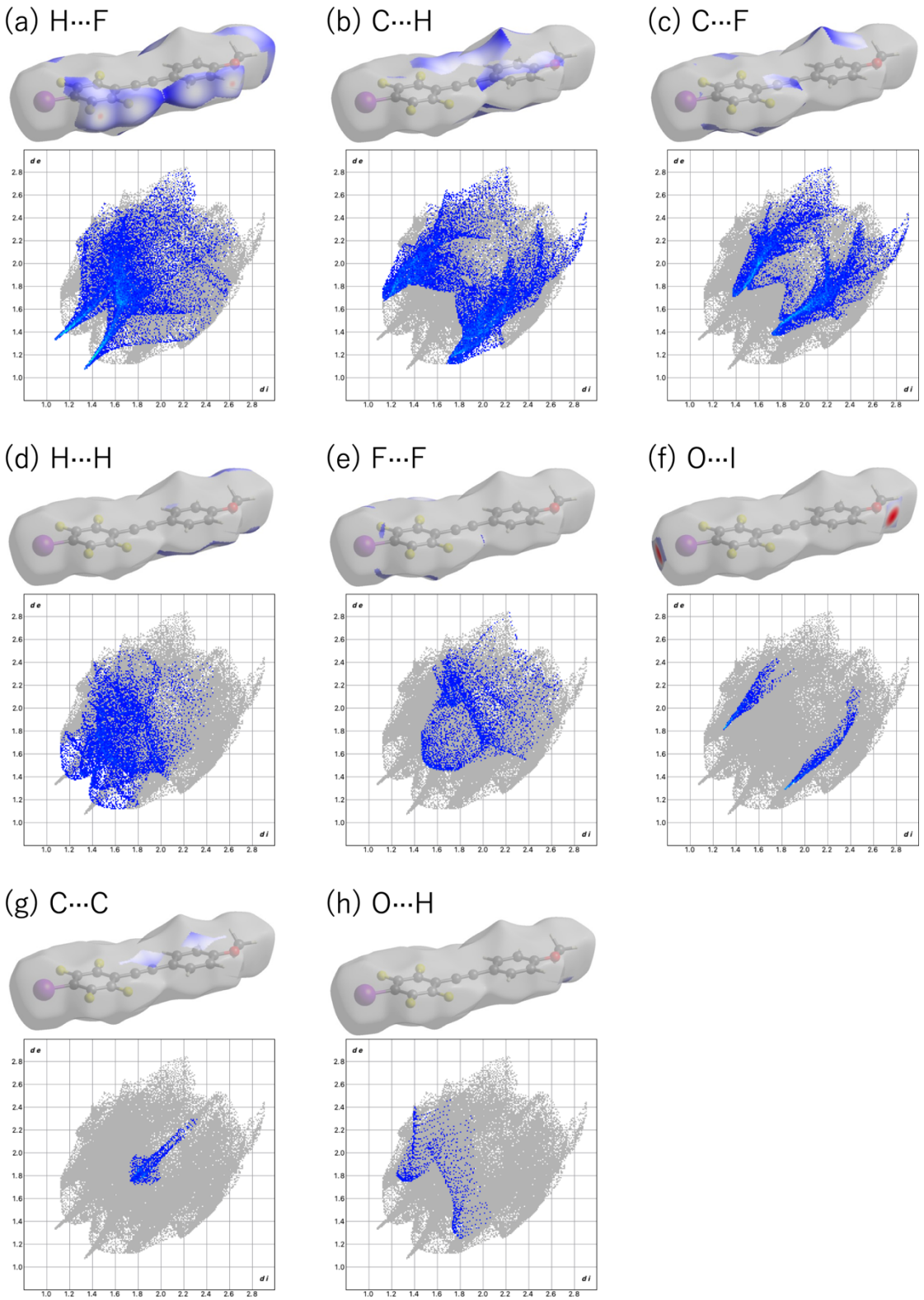

Fig. S14 Decomposed 2D Hirshfeld fingerprint plots for compound **1**, illustrating the contributions from the principal intermolecular contacts: (a) H···F, (b) C···H, (c) C···F, (d) H···H, (e) F···F, (f) O···I, (g) C···C, and (h) O···H. The Hirshfeld surfaces above each plot are mapped with d_{norm} to highlight the areas corresponding to each specific contact.

5. Quantum Chemical calculation

Using the Gaussian 16 software package (Revision C.01),[4] geometry optimisations were performed with the B3LYP and 6-31+G(d) basis set.

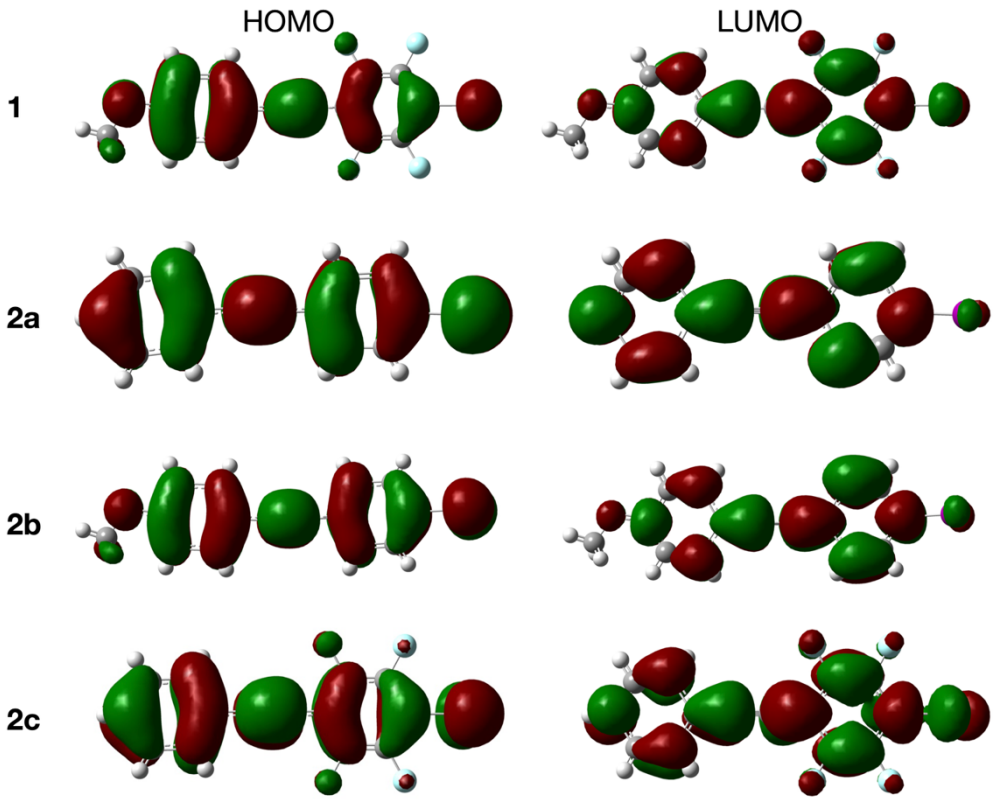

Fig. S15 Calculated frontier molecular orbitals (HOMO and LUMO) for compounds **1**, **2a**, **2b**, and **2c**. The orbitals were obtained from single-point DFT calculations at the B3LYP/6-31+G(d) level, using the molecular geometries extracted from their single-crystal X-ray structures.

[4] M. J. Frisch, G. W. Trucks, H. B. Schlegel, G. E. Scuseria, M. A. Robb, J. R. Cheeseman, G. Scalmani, V. Barone, G. A. Petersson, H. Nakatsuji, X. Li, M. Caricato, A. V. Marenich, J. Bloino, B. G. Janesko, R. Gomperts, B. Mennucci, H. P. Hratchian, J. V. Ortiz, A. F. Izmaylov, J. L. Sonnenberg, D. Williams-Young, F. Ding, F. Lipparini, F. Egidi, J. Goings, B. Peng, A. Petrone, T. Henderson, D. Ranasinghe, V. G. Zakrzewski, J. Gao, N. Rega, G. Zheng, W. Liang, M. Hada, M. Ehara, K. Toyota, R. Fukuda, J. Hasegawa, M. Ishida, T. Nakajima, Y. Honda, O. Kitao, H. Nakai, T. Vreven, K. Throssell, J. A. Montgomery Jr., J. E. Peralta, F. Ogliaro, M. J. Bearpark, J. J. Heyd, E. N. Brothers, K. N. Kudin, V. N. Staroverov, T. A. Keith, R. Kobayashi, J. Normand, K. Raghavachari, A. P. Rendell, J. C. Burant, S. S. Iyengar, J. Tomasi, M. Cossi, J. M. Millam, M. Klene, C. Adamo, R. Cammi, J. W. Ochterski, R. L. Martin, K. Morokuma, O. Farkas, J. B. Foresman and D. J. Fox, Gaussian16, revision, C. 01, *Gaussian Inc.*

Table S4 Calculated frontier orbital energy levels and energy gaps (ΔE) for compounds **1** and **2a–c**, obtained from DFT calculations on their single-crystal geometries.

	HOMO / eV	LUMO / eV	ΔE / eV
1	–6.118	–1.982	4.136
2a	–6.119	–1.623	4.496
2b	–5.753	–1.493	4.260
2c	–6.556	–2.173	4.383